Numerical simulation of diffusion MRI signals using an adaptive time-stepping method

Jing-Rebecca Li, Donna Calhoun, Cyril Poupon, Denis Le Bihan

Effcient Cartesian grid simulation tool for diffusion MRI

Jing-Rebecca Li Donna Calhoun Cyril Poupon Denis LeBihan

***Abstract*—The multiple-compartment Bloch-Torrey partial differential equation (PDE) can be used to model the bulk magnetization of a sample under the influence of a diffusion gradient. We present a simulation tool for diffusion MRI signals arising from complicated cellular geometries under the influence of an arbitrarily-shaped diffusion gradient that has low computational time and memory requirements. Our approach involves solving the Bloch-Torrey PDE by coupling a mass-conserving finite volume discretization in space with a stable time discretization using an explicit Runge-Kutta-Chebyshev method. We show simulation results for cellular geometries containing two and three compartments, with permeable and impermeable membranes, for nearly isotropic as well as anistropic diffusion, using the PGSE as well as OGSE sequences. This simulation tool has the advantage of producing reasonable accurate results in two and three dimensions for moderately complicated geometries in low computational time and without requiring intensive computing resources.**

***Index Terms*—Bloch-Torrey, partial differential equation (PDE), diffusion magnetic resonance imaging, finite volume.**

I. Introduction

BIOLOGICAL tissue is a heterogeneous medium, consisting of cells of various sizes and shapes distributed in the extra-cellular space. The intra-cellular compartment (the ensemble of all the cells) is separated from the extra-cellular compartment by the cell membranes, which permit water molecules to move from one compartment to the other. Diffusion magnetic resonance imaging is an imaging modality that subject the tissue to various magnetic fields and gives a measure of the average displacement of water molecules over a time period of milliseconds.

If the cell membranes do not permit the passage of water molecules, water diffusion is said to be 'restricted'. Restricted diffusion in the context of diffusion MRI is the subject of many papers, including [1], [2]. The analysis of restricted diffusion is simpler than the case of permeable membranes because analytical formulae for the solution of restricted diffusion are known for special geometries (sphere, cylinder, plane) [3].

If the cell membranes are permeable, analytical solutions are not known even for the special geometries above. In this case, researchers rely on numerical simulation as well as simplified models. Two examples of numerical simulation are Monte-Carlo simulations where random walkers mimic the behavior of concentrated densities of water molecules in a heterogeneous environment [4], [5], [6] and the numerical solution of the multiple compartment Bloch-Torrey equation [7], [8], [9].

In this paper, we take as the full model the two or three compartment Bloch-Torrey PDE, rather than Monte-Carlo simulation. All simulated signals are obtained by numerical solution the full Bloch-Torrey PDE. In the spatial discretization of the PDE, we conserved numerical fluxes across the interfaces, hence there is no numerical mass loss associated with this method. In the time discretization, we used the Runge-Kutta Chebyshev method[11], which is an explicit time stepping method, meaning no large matrices need to be inverted at each time step, and the allowed time step Δt is much larger than most commonly used methods (Euler or Crank-Nicolson time stepping, Monte-Carlo methods). In addition, the time step is adaptive: the code uses more time steps when problem needs it, namely, during the time when the gradient is turned on. This is all done automatically, based on the absolute and relative error tolerances on the computed residual, as requested by the user.

The paper is organized as follows. In Section II we describe the Bloch-Torrey PDE model. In Section III we describe our numerical method which couple a mass conserving finite volume discretization with the RKC time stepping method. In Section IV we show numerical results for nearly isotropic as well as anistropic diffusion for the PGSE and the cosine OGSE sequences. Section V contains our conclusions.

II. Two or three compartment Bloch Torrey PDE model

We model the magnetization in biological tissue due to a diffusion gradient at the voxel level by a multiple compartment Bloch-Torrey partial differential equation. We assume the tissue sample consists of n compartments: $\Omega^j, j = 1, \cdots, n$, each with a diffusion coefficient D^j, and $\bigcup_{j=1}^{n} \Omega^j = V$, where V is the voxel.

In biological tissue, it is often sufficient to consider a two-compartment, $n = 2$, or a three compartment, $n = 3$, model. In the two compartment model, one can consider the two compartments to be Ω^i and Ω^e, the ensemble of cells and the extra-cellular compartment, respectively. The cell membrane can be modelled by an infinitely thin permeable interface. In the three compartments model, the ensemble of membranes (possibly including a thick layer around) can be considered the third compartment, Ω^m.

If we assume some concentrated mass of water molecules located at $\mathbf{x}_0$ at $t = 0$, we want to find the magnetization at

J.-R. Li is with INRIA Saclay-Equipe DEFI CMAP, Ecole Polytechnique Route de Saclay, 91128, Palaiseau Cedex, France e-mail: jingrebecca.li@inria.fr

Donna Calhoun is with Department of Mathematics Boise State University 1910 University Dr. Boise, ID 83725-1555

Cyril Poupon and Denis LeBihan are NeuroSpin, CEA Saclay Center 91191 Gif-sur-Yvette Cedex FRANCE

time t due this initial density. Supposing the diffusion gradient with profile $f(t)$ and gradient vector $\mathbf{g} := \frac{\mathbf{q}}{\gamma}$, where γ is the gyromagnetic ratio, we use the Bloch Torrey PDE model in each compartment:

$$\frac{\partial m^j(\mathbf{x},t|\mathbf{x}_0,\mathbf{q})}{\partial t} = -\sqrt{-1}f(t)(\mathbf{q}\cdot\mathbf{x})\, m^j(\mathbf{x},t|\mathbf{x}_0,\mathbf{q}) + \nabla\cdot(D\nabla m^j$$
$$m^j(\mathbf{x},0|\mathbf{x}_0,\mathbf{q}) = \delta(\mathbf{x}-\mathbf{x}_0),\ \mathbf{x}\in\Omega^j.$$

The magnetization in Ω^j, $m^j(\mathbf{x},t,|\mathbf{x}_0,\mathbf{q})$, is a function of position and time, and depends on the parameters $\mathbf{x}_0$ and $\mathbf{q}$. The initial mass can be found anywhere in the voxel: $\mathbf{x}_0 \in \Omega^i \cup \Omega^e \cup \Omega^m$.

For the pulsed gradient spin echo (PGSE) sequence, the profile $f(t)$ (see Figure 1(a)) is:

$$f(t) = \begin{cases} 1, & 0 \le t \le \delta, \\ -1, & \Delta < t < t_{final} := \Delta + \delta. \end{cases}$$

For the cosine ocsillating gradient spin echo (OGSE) with frequency ω the profile (see Figure 1(b)) is:

$$f(t) = \begin{cases} \cos(2vt), & 0 \le t \le \delta, \\ -\cos(2v(t-\delta-\Delta)), & \Delta < t < t_{final} := \Delta + \delta, \end{cases},$$

The PDEs and the initial condition need to be supplemented by interface conditions where Ω^j and Ω^k come together. We denote the interface between Ω^j and Ω^k by Γ^{jk}. We will consider the case where all points on the interface touch only two compartments, i.e., if $n = 3$, there is not point where the three compartments come together. This is a reasonable assumption since the intra-cellular and the extra-cellular compartments will always seperated by the membrane in the three compartment model mentioned above. This way, the limiting value of the magnetization as $\mathbf{x}$ approaches $\mathbf{y} \in \Gamma^{jk}$ from Ω^j is simply $m^j(\mathbf{y},t,|\mathbf{x}_0,\mathbf{q})$ and it is $m^k(\mathbf{y},t,|\mathbf{x}_0,\mathbf{q})$ if the limit is approached from Ω^k.

One interface condition is the continuity of flux

$$D^j\left(\nabla m^j(\mathbf{y},t|\mathbf{x}_0,\mathbf{q})\cdot\mathbf{n}^j(\mathbf{y})\right) = -D^k\left(\nabla m^k(\mathbf{y},t|\mathbf{x}_0,\mathbf{q})\cdot\mathbf{n}^k(\mathbf{y})\right),\ \mathbf{y}\in\Gamma^{jk},$$

where $\mathbf{n}^j(\mathbf{y})$ and $\mathbf{n}^k(\mathbf{y})$ are the *outward*-point normals to Ω^j and Ω^k at $\mathbf{y}$, so in fact $\mathbf{n}^j(\mathbf{y}) = -\mathbf{n}^k(\mathbf{y})$. This ensures the conservation of magnetization.

The second interface condition is harder to formulate. In many papers it is

$$D^j\left(\nabla m^j(\mathbf{y},t|\mathbf{x}_0,\mathbf{q})\cdot\mathbf{n}^j(\mathbf{y})\right) = \kappa^{jk}\left(m^j(\mathbf{y},t|\mathbf{x}_0,\mathbf{q}) - m^k(\mathbf{y},t,|\mathbf{x}_0,\mathbf{q})\right),\ \mathbf{y}\in\Gamma^{jk}.$$

This incorporates a permeability coefficient κ^{jk} across Γ^{jk}. If $\kappa^{jk} = \infty$ then we have the simple continuity condition on m:

$$m^j(\mathbf{y},t|\mathbf{x}_0,\mathbf{q}) = m^k(\mathbf{y},t|\mathbf{x}_0,\mathbf{q}),\ \mathbf{y}\in\Gamma^{jk}.$$

A. Three compartment model

For simplicity, we assume the diffusion coefficients inside the cells and in the extra-cellular compartment are the same: $D^i = D^e = D^0$. In the three compartment model, where Ω^i is the intra-cellular compartment, Ω^e is the extra-cellular compartment, Ω^m is the membrane compartment, we have the following three PDEs:

$$\frac{\partial m^j(\mathbf{x},t|\mathbf{x}_0,\mathbf{q})}{\partial t} = -\sqrt{-1}f(t)(\mathbf{q}\cdot\mathbf{x})\, m^j(\mathbf{x},t|\mathbf{x}_0,\mathbf{q}) + \nabla\cdot(D^j\nabla m^j(\mathbf{x},t| \tag{1}$$

with the initial condition:

$$m^j(\mathbf{x},0|\mathbf{x}_0,\mathbf{q}) = \delta(\mathbf{x}-\mathbf{x}_0),\ \mathbf{x}\in\Omega^j,\ \mathbf{x}_0\in\Omega^i\cup\Omega^e\cup\Omega^m, \tag{2}$$

and interface conditions on the interface between the intra-cellular compartment and the membrane, and the interface between the extra-cellular compartment and the membrane:

$$D^0\left(\nabla m^j(\mathbf{y},t|\mathbf{x}_0,\mathbf{q})\cdot\mathbf{n}^j(\mathbf{y})\right) = -D^m\left(\nabla m^m(\mathbf{y},t|\mathbf{x}_0,\mathbf{q})\cdot\mathbf{n}^m(\mathbf{y})\right), \quad \mathbf{y}\in \tag{3}$$

$$m^j(\mathbf{y},t|\mathbf{x}_0,\mathbf{q}) = m^m(\mathbf{y},t|\mathbf{x}_0,\mathbf{q}), \quad \mathbf{y}\in \tag{4}$$

We have assumed that magnetization is continuous across the interfaces, i.e., the permeability is infinite across them.

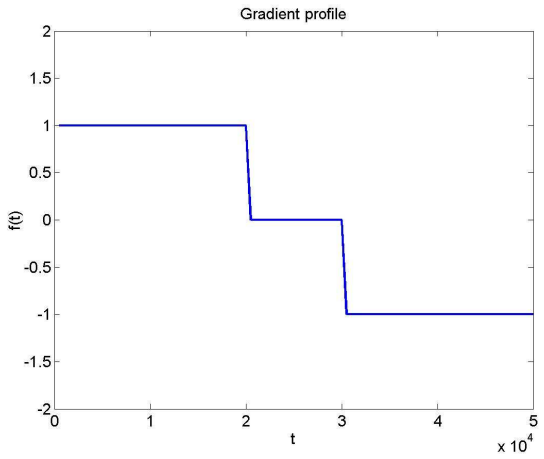

(a) PGSE $\delta = 20000\mu s$, $\Delta = 30000\mu s$

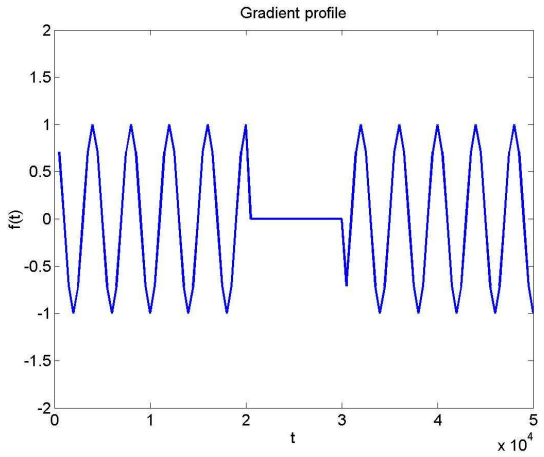

(b) Cosine OGSE $\delta = 20000\mu s$, $\Delta = 30000\mu s$, $\omega = 5$

Fig. 1. Two example diffusion sequences.

B. Two compartment model with finite permeability

In the two compartment model, the membrane compartment Ω^m is replaced by an infinitely thin interface Γ^{ie}, with a finite permeability coefficient κ. We have the following two PDEs:

$$\frac{\partial m^j(\mathbf{x},t|\mathbf{x}_0,\mathbf{q})}{\partial t} = -\sqrt{-1}f(t)(\mathbf{q}\cdot\mathbf{x})\, m^j(\mathbf{x},t|\mathbf{x}_0,\mathbf{q}) + \nabla\cdot(D^0\nabla m^j(\mathbf{x},t|\mathbf{x}_0,\mathbf{q})), \mathbf{x}\in\Omega^j, \quad j=i,e \tag{5}$$

with the initial condition:

$$m^j(\mathbf{x},0|\mathbf{x}_0,\mathbf{q}) = \delta(\mathbf{x}-\mathbf{x}_0),\ \mathbf{x}\in\Omega^j,\ \mathbf{x}_0\in\Omega^i\cup\Omega^e, \tag{6}$$

and interface conditions on the interface between the intra-cellular compartment and the extra-cellular compartment:

$$\left(\nabla m^i(\mathbf{y},t|\mathbf{x}_0,\mathbf{q})\cdot\mathbf{n}^i(\mathbf{y})\right) = -\left(\nabla m^e(\mathbf{y},t|\mathbf{x}_0,\mathbf{q})\cdot\mathbf{n}^e(\mathbf{y})\right), \quad \mathbf{y}\in\Gamma^{ie} \tag{7}$$

$$D^0\left(\nabla m^i(\mathbf{y},t|\mathbf{x}_0,\mathbf{q})\cdot\mathbf{n}^i(\mathbf{y})\right) = \kappa\left(m^i(\mathbf{y},t|\mathbf{x}_0,\mathbf{q}) - m^e(\mathbf{y},t,|\mathbf{x}_0,\mathbf{q})\right), \quad \mathbf{y}\in\Gamma^{ie} \tag{8}$$

An approximate way to relate the two compartment model and the three compartment model is that the permeability coefficient in the two compartment model is approximately $\kappa\approx\frac{D^m}{h}$, where D^m is the diffusion coefficient in Ω^m and h is the thickness of the membrane layer in the three compartment model.

C. The DMRI signal

The 'total' signal attenuation (non-normalized) is then

$$\Psi(\mathbf{q},t) = \sum_j\sum_k \int_{\mathbf{x}_0\in\Omega^k} \Psi^j(\mathbf{q},t|\mathbf{x}_0)d\mathbf{x}_0, \tag{9}$$

where

$$\Psi^j(\mathbf{q},t|\mathbf{x}_0) = \int_{\mathbf{x}\in\Omega^j} m^j(\mathbf{x},t|\mathbf{x}_0,\mathbf{q})\, d\mathbf{x}, \tag{10}$$

with $j,k\in\{i,e\}$ in the two compartment model and $j,k\in\{i,e,m\}$ in the three compartment model. The total signal sums over compartments and over initial conditions.

From the DMRI signal attenuation, two quantities can be obtained: the ADC (apparent diffusion coefficient) and the Kurtosis. The ADC and the Kurtosis are defined as the first (negated) and second order terms of the Taylor expansion in b-value of the logarithm of the DMRI signal attenuation:

$$\log\{\Psi(b)\} = 0 - ADC * b + KUR * b^2 + O(b^3). \tag{11}$$

where the b-value depends on $\mathbf{q}$ and t and is defined as:

$$b(\mathbf{q},t) = \|\mathbf{q}\|^2\int_0^t du\left(\int_s^u f(s)ds\right)^2,$$

$f(s)$ being the diffusion gradient profile.

III. PDE DISCRETIZATION

We describe a simple numerical method that solves the Bloch-Torrey equation in three dimensions that is reasonably accurate, fast, and has low memory requirements. All the computations described in this paper on performed on a Dell personal laptop computer (Latitude E6410, 2.8GHz Intel Core i7 processor) with computational time of tens of minutes per bvalue.

In the following vectors in three dimensions will be printed in bold, such as $\mathbf{x}$. The three components of the vector will not be bold, i.e., $\mathbf{x}=(x,y,z)$.

A. Cartesian discretization grid

We use a rectangular computational domain $M=[a,b]\times[c,d]\times[e,f]$ that contains a configuration of cells. Because we are only interested in getting the signal with moderate accuracy (we can tolerate error of up to 1 or 2 percent), we decided to discretize M by rectangular parallelpipeds, rather than more general tetrahedrals. Thus, the cells in our discretizations will have jagged membranes. This greatly simplies the spatial discretization of the multiple compartment PDE because the interface between Ω^j and Ω^k are made up only of rectangles that are parallel to one of the coordinate planes.

Let

$$\Delta x = \frac{b-a}{N}, \quad \Delta y = \frac{c-d}{P}, \quad \Delta z = \frac{e-f}{Q},$$

we denote by $\{x_1,\cdots x_N\}$ and $\{y_1,\cdots,y_P\}$ and $\{z_1,\cdots,z_Q\}$ our discretization points in the x, y, z coordinates, respectively:

$$x_i = a+i\Delta x-\Delta x/2, \quad y_j = c+j\Delta y-\Delta y/2, \quad z_k = e+k\Delta z-\Delta z/2.$$

A typical element will be the rectangular parallelpiped

$$R_{ijk}\equiv[x_i-\Delta x/2, x_i+\Delta x/2]\times[y_j-\Delta y/2, y_j+\Delta y/2]\times[z_k-\Delta z/2, z_k+\Delta$$

centered at $\mathbf{x}_{ijk}\equiv\{x_i,y_j,z_k\}$. On each element R_{ijk}, the diffusion coefficient will be constant and we denote the value by D_{ijk}. For the two compartment model the value of D_{ijk} is always D^0. For the three compartment model, the value of D_{ijk} is either D^0 or D^m.

B. Conservation of mass

Let $\overline{m}_{ijk}(t)$ be the volume average in R_{ijk} of the magnetization $m(\mathbf{x},t)$:

$$\overline{m}_{ijk}(t)\equiv\frac{1}{\Delta x\Delta y\Delta z}\int_{R_{ijk}} m(\mathbf{x},t)d\mathbf{x}.$$

Let $\overline{\mathbf{x}m}_{ijk}(t)$ be the following volume average:

$$\overline{\mathbf{x}m}_{ijk}(t)\equiv\frac{1}{\Delta x\Delta y\Delta z}\int_{R_{ijk}}\mathbf{x}\, m(\mathbf{x},t)\, d\mathbf{x}.$$

We integrate the Bloch-Torrey PDE over R_{ijk}:

$$\int_{R_{ijk}}\frac{\partial m(\mathbf{x},t)}{\partial t}d\mathbf{x} = -\sqrt{-1}f(t)\int_{R_{ijk}}(\mathbf{q}\cdot\mathbf{x})\, m(\mathbf{x},t)d\mathbf{x} + \int_{R_{ijk}}\nabla\cdot(D(\mathbf{x})$$

$$\frac{\partial\overline{m}_{ijk}(t)}{\partial t} = -\sqrt{-1}f(t)(\mathbf{q}\cdot\overline{\mathbf{x}m}_{ijk}(t)) + \frac{1}{\Delta x\Delta y\Delta z}\oint_{\partial R_{ijk}} D(\mathbf{x})$$

and make the approximation:

$$\frac{\partial \overline{m}_{ijk}(t)}{\partial t} \approx -\sqrt{-1} f(t)(\mathbf{q}\cdot\mathbf{x}_{ijk})\,\overline{m}_{ijk}(t) + \frac{1}{\Delta x\Delta y\Delta z}\oint_{\partial R_{ijk}} D_{ijk}\nabla m(\mathbf{x},t)\cdot\mathbf{n}dS,$$
$$\approx -\sqrt{-1} f(t)(\mathbf{q}\cdot\mathbf{x}_{ijk})\,\overline{m}_{ijk}(t) + L_{ijk}(t),$$

where the flux is

$$L_{ijk}(t) = D_{ijk}\left(\sum \pm \frac{\frac{\partial m}{dx}(x_i \pm \Delta x/2, y_j, z_k, t)}{\Delta x} + \sum \pm \frac{\frac{\partial m}{dy}(x_i, y_j \pm \Delta y/2, z_k, t)}{\Delta y} + \sum \pm \frac{\frac{\partial m}{dz}(x_i, y_j, z_k \pm \Delta z/2, t)}{\Delta z}\right),$$

To compute the quantities in the previous equation, we need an approximation to the first order spatial derivatives at the faces of R_{ijk}.

For concreteness, we discuss the x-derivative. Let $F_{i+\frac{1}{2},jk}$ be the right face of R_{ijk}. If the diffusion coefficient is continuous in x at $\left(x_{i+\frac{1}{2}}, y_j, z_k\right)$, $D_{ijk} = D_{i+1,jk}$, then m and $\frac{\partial m}{\partial x}$ are too, so the standard centered-difference approximation can be used:

$$D_{ijk}\frac{\partial m}{dx}\left(x_{i+\frac{1}{2}}, t\right) \approx \frac{1}{\Delta x} D^*_{i+\frac{1}{2},jk}\left(m(x_{i+1},t), -m(x_i,t)\right),$$

where

$$D^*_{i+\frac{1}{2},jk} = D_{ijk}. \tag{12}$$

We suppressed the arguments y_j, z_k above to shorten the formula.

If the diffusion coefficient is not continous in x at $\left(x_{i+\frac{1}{2}}, y_j, z_k\right)$, $D_{ijk} \neq D_{i+1,jk}$, then there would be two different limit values of $\frac{\partial m}{\partial x}$ and possibly m as x approaches the face $F_{i+\frac{1}{2},j,k}$ from left and from the right. Since the face $F_{i+\frac{1}{2},j,k}$ is to the right of the element R_{ijk} we will need the left hand limit of m and make the following approximation for the flux on $F_{i+\frac{1}{2},j,k}$:

$$D_{ijk}\frac{\partial m^-}{dx}\left(x_{i+\frac{1}{2}}, t\right) \approx \frac{D_{ijk}}{\Delta x/2}\left(m^-(x_{i+\frac{1}{2}}, t) - m(x_i, t)\right). \tag{13}$$

We must solve for the interface values $m^-\left(x_{i+\frac{1}{2}}, y_j, z_k, t\right)$ and $m^+\left(x_{i+\frac{1}{2}}, y_j, z_k, t\right)$ to the left and right of $F_{i+\frac{1}{2},j,k}$. To solve for them, we use the two interface conditions. The first comes from flux continuity:

$$D_{ijk}\frac{1}{\Delta x/2}\left(m^-(x_{i+\frac{1}{2}}, t) - m(x_i, t)\right) = D_{i+1,jk}\frac{1}{\Delta x/2}\left(m(x_{i+1}, t) - m^+(x_{i+\frac{1}{2}}, t)\right) \tag{14}$$

For the three compartment model, the second condition comes from the continuity of the concentration

$$m^-(x_{i+\frac{1}{2}}, t) = m^+(x_{i+\frac{1}{2}}, t). \tag{15}$$

The solution of (14-15) is

$$m^+(x_{i+\frac{1}{2}}, t) = m^-(x_{i+\frac{1}{2}}, t) = \frac{D_{i+1,jk}m(x_{i+1}, t) + D_{ijk}m(x_i, t)}{D_{i+1,jk} + D_{ijk}}.$$

Then the flux term in (13) is

$$D_{ijk}\frac{\partial m^-}{dx}(x_{i+\frac{1}{2}}, t) \approx D^*_{i+\frac{1}{2},jk}\frac{1}{\Delta x}\left(m(x_{i+1}, t) - m(x_i, t)\right),$$

where

$$D^*_{i+\frac{1}{2},jk} = \frac{1}{\frac{1}{2}\left(\frac{1}{D_{i+1,jk}} + \frac{1}{D_{ijk}}\right)}. \tag{16}$$

For the two compartment model, the second condition comes from the permeability condition:

$$D_{ijk}\frac{1}{\Delta x/2}\left(m^-(x_{i+\frac{1}{2}}, t) - m(x_i, t)\right) = \kappa\left(m^+(x_{i+\frac{1}{2}}, t) - m^-(x_{i+\frac{1}{2}}, t)\right), \tag{17}$$

After solving (14 and 17) the flux term in (13) becomes

$$D_{ijk}\frac{\partial m^-}{dx}(x_{i+\frac{1}{2}}, t) \approx D^*_{i+\frac{1}{2},jk}\frac{1}{\Delta x}\left(m(x_{i+1}, t) - m(x_i, t)\right),$$

where

$$D^*_{i+\frac{1}{2},jk} = \frac{1}{\left(\frac{1}{2}\left(\frac{1}{D(x_{i+1})} + \frac{1}{D(x_i)}\right) + \frac{1}{\kappa\Delta x}\right)}. \tag{18}$$

The final discretization formula is:

$$\frac{\partial \overline{m}_{ijk}(t)}{\partial t} \approx -\sqrt{-1} f(t)(\mathbf{q}\cdot\mathbf{x}_{ijk})\,\overline{m}_{ijk}(t) + \frac{1}{\Delta x^2}\left(D^*_{i+\frac{1}{2},jk}\left(\overline{m}_{i+1,j,k} - \overline{m}\right.\right.$$
$$+ \frac{1}{\Delta y^2}\left(D^*_{i,j+\frac{1}{2},k}\left(\overline{m}_{i,j+1,k} - \right.\right.$$
$$+ \frac{1}{\Delta z^2}\left(D^*_{ij,k+\frac{1}{2}}\left(\overline{m}_{ij,k+1}, t\right) - \right. \tag{19}$$

where D^* is given by (12) at a continous face, at a discontinuous face, D^* is given by (16) for the three compartment model and it is given by (18) for the two compartment model.

The spatial discretization in (19) gives rise to a system of ODEs in time which we will solve by a time stepping method described in Section III-D.

C. Pseudo-periodic boundary condition

We need to impose boundary conditions on the boundary of the computational domain M. We chose to mimic the effect of an infinite domain where M repeated infinitely in all three coordinate directions. When we want to study the effect of volume fraction or cell size on the signal, we may want to put only one or a few cells in M and the total signal will be due to an infinite number of cells placed periodically in x, y and z directions. When we want to study the effect of a heterogeneous configuration of cells, we will put a large number of cells of different shapes and sizes in M. In latter case, it is still more reasonable to assume the infinite periodic extension outside of M then to impose, for example, simple Neumann (prescribed flux) or Dirichlet (prescribed concentration) boundary conditions on the faces of M. This is because we do not know the exact flux or concentration at ∂M, but we do know that there are cells outside of M. In the case where we put only a localized initial source at the center of M, and simulate only for times where the concentration on ∂M is negligible, then it does not matter what boundary condition one imposes on ∂M.

The boundary conditions we impose are the following pseudo-periodic boundary conditions:

$$\overline{m}_{1jk}(t) = \overline{m}_{N+1,jk}(t)e^{i\,q_1\,(b-a)\,\theta(t)}, \quad \frac{\partial}{\partial x}\overline{m}_{1jk}(t) = \frac{\partial}{\partial x}\overline{m}_{N+1,jk}(t)e^{i\,q_1\,(b-a)\,\theta(t)} \tag{20}$$

$$\overline{m}_{i1k}(t) = \overline{m}_{i,P+1,k}(t)e^{i\,q_2\,(c-d)\,\theta(t)}, \quad \frac{\partial}{\partial x}\overline{m}_{i,1,k}(t) = \frac{\partial}{\partial x}\overline{m}_{i,P+1,k}(t)e^{i\,q_2\,(c-d)\,\theta(t)} \tag{21}$$

$$\overline{m}_{ij1}(t) = \overline{m}_{ij,Q+1}(t)e^{i\,q_3\,(e-f)\theta(t)}, \quad \frac{\partial}{\partial x}\overline{m}_{ij1}(t) = \frac{\partial}{\partial x}\overline{m}_{ij,Q+1}(t)e^{i\,q_3\,(e-f)\,\theta(t)} \tag{22}$$

where

$$\theta(t) = \int_0^t f(s)\,ds, \tag{23}$$

where $f(t)$ is the gradient profile.

D. RKC time stepping method

In the previous sections we discretized the Bloch-Torrey PDE into the systems of ODEs in (19). Now we solve the ODEs using a family of multiple-stage Runge-Kutta-Chebyshev (RKC) formulae [11]. The RKC method was originally conceived to solve large systems of ODEs coming from the spatial discretization of diffusion-dominated PDEs, which is exactly the case of our finite volume discretizion of the Bloch-Torrey PDE. For this problem, the RKC method performs much better than simpler time stepping methods such as forward or backward Euler methods.

The implementation of the RKC method comes from the publicly available Fortran code downloaded from http://www.netlib.org/ode/rkc.f. In this implementation, at each requested time point t and requested time step Δt, the most efficient time stepping formula and time sub-steps are chosen so that the solution at $t + \Delta t$ of the ODE in (19) is obtained within a requested residual tolerance and with only a few vectors of storage.

IV. Numerical results

We show numerical results for nearly isotropic as well as anistropic diffusion, for the PGSE as well as the cosine OGSE sequences.

In all the simulations, we set the time stepping residual tolerance at $tol = 1 \times 10^{-3}$ and requested the RKC code to return an answer to the system of ODEs in (19) at each time step of $\Delta t = 2500\mu s = 2.5ms$. The RKC code automatically determined the most efficient time stepping formulae going from t_n to $t_n + \Delta t$ that provides an answer within the residual tolerance. Thus, to simulate $50ms$, only 100 RKC time steps are needed. In the examples below, we will show the number of function evaluations (evaluation of the right hand side of (19)) at each RKC time step for different diffusion sequences and gradient magnitudes.

A. Three compartments

In Figure 2 we show a three compartment example. The cells are spheres placed periodically in the three coordinate directions. Each sphere has outer radius $R = 4.8\mu m$ and a membrane layer of thickness $h = 0.2\mu m$. The membrane layer Ω^m makes up 5% of the total volume. The distance between the spheres is $L = 10\mu m$ in all three coordinate directions. We illustrate the cellular geometry in Figure 2(a) where the membrane compartment is light colored.

Our computational domain is a cube $M = [-L/2, L/2]^3$. The spatial discretization of M is $N = 50$, $P = 50$, $Q = 50$ in the x, y, and z coordinates, respectively. The RKC time step is $\Delta t = 500\mu s = 0.5ms$.

We chose the intrinsic diffusion coefficient to be $D^0 = 2.8\times 10^{-3}\frac{\mu m^2}{\mu s}$ and the membrane diffusion coefficient $D^m = \kappa h$, where the permeability coefficient we want to simulate is $\kappa = 1 \times 10^{-4}\frac{\mu m}{\mu s}$. In Figure 2(c) we show the normalized signal at five different b-values for the PGSE sequence with $\delta = 20000\mu s$ and $\Delta = 30000\mu s$. We see the $ADC = 1.47\times 10^{-3}\frac{\mu m^2}{\mu s}$, which is 50% of D^0. In Figure 2(b) we show the number of function evaluations (evaluation of the right hand side of (19)) at each time step $\Delta t = 500\mu s = 0.5ms$. For the lowest gradient magnitude $\|\mathbf{g}\| = 0$, the number of evaluations is few than 10. For the highest gradient magnitude corresponding to a bvalue of $b = 3733$, the number of evaluations per Δt is between 50 and 100. In Figure 2(d) we show the computational time for each bvalue. At $b = 0$ the computational time is 10 seconds. At the highest $b = 3733$, the computational time is 1.5 minutes.

B. Various PGSE sequences

In Figure 3 we show a two compartment example. The cells are cubes placed periodically in the three coordinate directions. Each sphere has outer radius $R = 4.9\mu m$. There is no membrane layer. The intra-cellular volume fraction is 94%. The distance between the cells is $L = 10\mu m$ in all three coordinate directions. We illustrate the cellular geometry in Figure 3(a) where the intra-cellular compartment is dark colored.

Our computational domain is a cube $M = [-L/2, L/2]^3$, where $L = 10\mu m$. Because the cells are very close to each other, we have to use a spatial discretization of $N = 100$, $P = 100$, $Q = 100$ in the x, y, and z coordinates, respectively, to be able to resolve the space between the cells. We chose the intrinsic diffusion coefficient to be $D^0 = 2.8 \times 10^{-3}\frac{\mu m^2}{\mu s}$ and the permeability coefficient to be $\kappa = 1 \times 10^{-4}\frac{\mu m}{\mu s}$. In Figure 3(c) we show the normalized signals for three PGSE sequences: with

1) $\delta = 20000\mu s, \quad \Delta = 30000\mu s,$
2) $\delta = 30000\mu s, \quad \Delta = 40000\mu s,$
3) $\delta = 50000\mu s, \quad \Delta = 50000\mu s,$

respectively. We see the simulated $ADC = 0.7 \times 10^{-3}\frac{\mu m^2}{\mu s}, 0.68\times 10^{-3}\frac{\mu m^2}{\mu s}, 0.67\times 10^{-3}\frac{\mu m^2}{\mu s}$, are close to each other and they are lower than for the spherical cells in Figure 2 due to a higher intra-cellular volume fraction. We also see that the Kurtosis is quite different for these three sequences,

they are $KUR = 0.77 \times 10^{-7} \frac{\mu m^2}{\mu s}^2, 0.6 \times 10^{-7} \frac{\mu m^2}{\mu s}^2, 0.46 \times 10^{-7} \frac{\mu m^2}{\mu s}^2$, respectively. In Figure 3(b) we show the number of function evaluations at each time step $\Delta t = 500\mu s = 0.5ms$ for the third diffusion sequence: $\delta = 50000\mu s$ and $\Delta = 50000\mu s$. For the lowest gradient magnitude $\|\mathbf{g}\| = 0$, the number of evaluations is fewer than 10. For the highest gradient magnitude corresponding to a bvalue of $b = 33333$, the number of evaluations per time step is between 100 and 200. In Figure 3(d) we show the computational time for each bvalue. At $b = 0$ the computational time is 5 minutes. At the highest $b = 33333$, the computational time is 50 minutes.

C. Cosine OGSE sequences

In Figure 4 we show a two compartment example. The cells are cubes placed periodically in the three coordinate directions. Each sphere has outer radius $R = 4.8\mu m$. There is no membrane layer. The intra-cellular volume fraction is 88%. The distance between the cells is $L = 10\mu m$ in all three coordinate directions. We illustrate the cellular geometry in Figure 4(a) where the intra-cellular compartment is dark colored.

Our computational domain is a cube $M = [-L/2, L/2]^3$, where $L = 10\mu m$. We used a spatial discretization is $N = 50$, $P = 50$, $Q = 50$ in the x, y, and z coordinates. We chose the intrinsic diffusion coefficient to be $D^0 = 2.8 \times 10^{-3} \frac{\mu m^2}{\mu s}$ and the permeability coefficient to be $\kappa = 1 \times 10^{-4} \frac{\mu m}{\mu s}$. In Figure 4(c) we show the normalized signals for four sequences with $\delta = 20000\mu s$ and $\Delta = 30000\mu s$. The first sequence is PGSE, the last three are cosine OGSE, with a frequency of $\omega = 0.5$, 1, and 5, respectively. The cosine OGSE sequence with frequence $\omega = 5$ is shown in Figure 4(b). There are five full periods each in the time intervals $[0, \delta]$ and $[\Delta, \Delta + \delta]$. We see the simulated $ADC = 0.79 \times 10^{-3} \frac{\mu m^2}{\mu s}, 0.93 \times 10^{-3} \frac{\mu m^2}{\mu s}, 1.29 \times 10^{-3} \frac{\mu m^2}{\mu s}, 2.17 \times 10^{-3} \frac{\mu m^2}{\mu s}$, approach the intrinsic value $D^0 = 2.8 \times 10^{-4} \frac{\mu m^2}{\mu s}$ as the frequence ω increases. For PGSE, we see that when we decreased the intra-cellular volume fraction to 94% of the previous example to 88%, the ADC increased from $0.7 \times 10^{-3} \frac{\mu m^2}{\mu s}$ to $0.79 \times 10^{-3} \frac{\mu m^2}{\mu s}$, an increase of 13%, consistent with experimental findings []. In Figure 4(b) we show the number of function evaluations at each time step $\Delta t = 500\mu s = 0.5ms$ for the cosine OGSE diffusion sequence with $\omega = 5$. For the lowest gradient magnitude $\|\mathbf{g}\| = 0$, the number of evaluations is few than 10. For the highest gradient magnitude corresponding to a bvalue of $b = 3.5$, the number of evaluations per time step is between 90 and 130 during the time the gradient is turned on, and it is around 50 during the time the gradient is turned off, namely, on $[\delta, \Delta]$. In Figure 4(d) we show the computational time for each bvalue. At $b = 0$ the computational time is 30 seconds. At the highest $b = 3.5$, the computational time is 3 minutes.

D. Cells with irregular shape

In Figure 5 we show a two compartment example with cells of an irregular shape: they are spheres with ridges on the surface. The cells are placed periodically in the three coordinate directions. The intra-cellular volume fraction is 64%. The distance between the cells is $L = 10\mu m$ in all three coordinate directions. We illustrate the cellular geometry in Figure 5(a) where the intra-cellular compartment is dark colored.

Our computational domain is a cube $M = [-L/2, L/2]^3$, where $L = 10\mu m$. Because the cells are very close to each other, we use a spatial discretization of $N = 100$, $P = 100$, $Q = 100$ in the x, y, and z coordinates, respectively. We chose the intrinsic diffusion coefficient to be $D^0 = 2.8 \times 10^{-3} \frac{\mu m^2}{\mu s}$ and the permeability coefficient to be $\kappa = 1 \times 10^{-4} \frac{\mu m}{\mu s}$. In Figure 5(c) we show the normalized signal for the PGSE sequence with $\delta = 20000\mu s$ and $\Delta = 30000\mu s$. We see the simulated ADC is $ADC = 1.12 \times 10^{-3} \frac{\mu m^2}{\mu s}$. In Figure 5(b) we show that the number of function evaluations for each time step $\Delta t = 500\mu s = 0.5ms$ is between 100 and 200 at the highest bvalue $b = 3733$. In Figure 5(d) we show the computational time for each bvalue. At $b = 0$ the computational time is 5 minutes. At the highest $b = 3733$, the computational time is 35 minutes.

In Figure 6 we removed the spheres and just left the ridges as the cells, which form a kind of network in the extra-cellular space. See Figure 6(a) for this intra-cellular network (colored dark). The intra-cellular volume fraction is reduced from 64% to 39% from the previous example. In Figure 6(c) we show the normalized signal for the PGSE sequence with $\delta = 20000\mu s$ and $\Delta = 30000\mu s$. We see the simulated ADC is $ADC = 1.04 \times 10^{-3} \frac{\mu m^2}{\mu s}$, even lower than the previous example. This is because in the previous example, the large spheres at the center of the cells made it easier for water to diffuse from one cell to another. The diffusion is more difficult when the cells are thin tubes as in this example. The number of function evaluations and computational time are about the same as the previous example.

E. Anistropic diffusion

In Figure 7 we show a two compartment example of anistropic diffusion. The cells are cylinders with rectangular cross-section. They are placed in alternating layers: parallel to the x-axis in the even layers and parallel to the y-axis in the odd layers (see Figure 7(a), the intra-cellular compartment is dark). Our computational domain is $M = [-80/2, 80/2] \times [-40/2, 40/2] \times [-20/2, 20/2]$. The intra-cellular volume fraction is 62%. The spatial discretization is $N = 160$, $P = 80$, $Q = 40$ in the x, y, and z coordinates, respectively. We chose the intrinsic diffusion coefficient to be $D^0 = 2.8 \times 10^{-3} \frac{\mu m^2}{\mu s}$ and the permeability coefficient to be $\kappa = 1 \times 10^{-4} \frac{\mu m}{\mu s}$. In Figure 7(c) we show the normalized signal for the PGSE sequence with $\delta = 20000\mu s$ and $\Delta = 30000\mu s$ in four different directions: $dir = \{1,0,0\}, \{0,1,0\}, \{0,0,1\}, \{1,3,1\}$. We see the simulated ADCs are $ADC = 2 \times 10^{-3} \frac{\mu m^2}{\mu s}$, $ADC = 1.51 \times 10^{-3} \frac{\mu m^2}{\mu s}$, $ADC = 0.65 \times 10^{-3} \frac{\mu m^2}{\mu s}$, $ADC = 1.48 \times 10^{-3} \frac{\mu m^2}{\mu s}$, respectively. This is as expected because the layers are the most dense in the z-direction, making diffusion most difficult in that direction. On the other hand, the cylinders are the most sparsely packed in the x-direction, hence the ADC

is the highest in the direction $dir = \{1, 0, 0\}$. In Figure 7(b) we show the number of function evaluations at each time step for $dir = \{1, 0, 0\}$. It is between 20 and 40. In Figure 7(d) we show the computational time for each bvalue, it is about 2 minutes per bvalue.

V. Conclusions

We presented a numerical method to solve the Bloch-Torrey partial differential equation in multiple diffusion compartments to simulate the bulk magnetization of a sample under the influence of a diffusion gradient. We coupled a mass-conserving finite volume discretization in space with a stable time discretization using an explicit Runge-Kutta-Chebyshev method. We are able to solve the Bloch-Torrey PDE in multiple compartments for an arbitrary diffusion sequence with reasonable accuracy for moderately complicated geometries in computational time that is on the order of tens of minutes per bvalue on a laptop computer. We were able to simulated DMRI signals for nearly isotropic as well as anistropic diffusion, for the PGSE as well as cosine OGSE sequences. We also show that this numerical method can be used to estimate the parameters that go into analytical models of DMRI signal such as the Karger model.

Appendix A
Proof of the First Zonklar Equation

Appendix one text goes here.

Appendix B

Appendix two text goes here.

Acknowledgment

The authors would like to thank...

References

[1] J. Pfeuffer, U. Flgel, W. Dreher, and D. Leibfritz, "Restricted diffusion and exchange of intracellular water: theoretical modelling and diffusion time dependence of 1h nmr measurements on perfused glial cells," *NMR in Biomedicine*, vol. 11, no. 1, pp. 19–31, 1998. [Online]. Available: http://dx.doi.org/10.1002/(SICI)1099-1492(199802)11:1⟨19::AID-NBM499⟩3.0.CO;2-O

[2] D. S. Grebenkov, "Pulsed-gradient spin-echo monitoring of restricted diffusion in multilayered structures: Challenges and solutions," *AIP Conf. Proc.*, vol. 1330, no. 1, pp. 65–68, Mar. 2011. [Online]. Available: http://dx.doi.org/10.1063/1.3562234

[3] J. Crank, *The mathematics of diffusion*, 2nd ed. Clarendon Press, Oxford, 1975.

[4] D. C. Alexander, "A general framework for experiment design in diffusion mri and its application in measuring direct tissue-microstructure features," *Magnetic Resonance in Medicine*, vol. 60, no. 2, pp. 439–448, 2008. [Online]. Available: http://dx.doi.org/10.1002/mrm.21646

[5] G. T. Balls and L. R. Frank, "A simulation environment for diffusion weighted mr experiments in complex media," *Magn. Reson. Med.*, vol. 62, no. 3, pp. 771–778, 2009. [Online]. Available: http://dx.doi.org/10.1002/mrm.22033

[6] M. Hall and D. Alexander, "Convergence and parameter choice for monte-carlo simulations of diffusion mri," *Medical Imaging, IEEE Transactions on*, vol. 28, no. 9, pp. 1354 –1364, Sept. 2009.

[7] S. N. Hwang, C.-L. Chin, F. W. Wehrli, and D. B. Hackney, "An image-based finite difference model for simulating restricted diffusion," *Magnetic Resonance in Medicine*, vol. 50, no. 2, pp. 373–382, 2003. [Online]. Available: http://dx.doi.org/10.1002/mrm.10536

[8] J. Xu, M. Does, and J. Gore, "Numerical study of water diffusion in biological tissues using an improved finite difference method." *Physics in medicine and biology*, vol. 52, no. 7, pp. –, Apr. 2007. [Online]. Available: http://view.ncbi.nlm.nih.gov/pubmed/17374905

[9] K. D. Harkins, J.-P. Galons, T. W. Secomb, and T. P. Trouard, "Assessment of the effects of cellular tissue properties on adc measurements by numerical simulation of water diffusion," *Magn. Reson. Med.*, vol. 62, no. 6, pp. 1414–1422, 2009. [Online]. Available: http://dx.doi.org/10.1002/mrm.22155

[10] J. Karger, H. Pfeifer, and W. Heinik, "Principles and application of self-diffusion measurements by nuclear magnetic resonance," *Advances in magnetic resonance*, vol. 12, pp. 1–89, 1988.

[11] B. P. Sommeijer, L. F. Shampine, and J. G. Verwer, "Rkc: An explicit solver for parabolic pdes," *Journal of Computational and Applied Mathematics*, vol. 88, no. 2, pp. 315–326, Mar. 1998. [Online]. Available: http://www.sciencedirect.com/science/article/B6TYH-3W0G0R4-12/2/96d3aca02fea5e5bcb582c862e1b3945

[12] E. Fieremans, D. S. Novikov, J. H. Jensen, and J. A. Helpern, "Monte carlo study of a two-compartment exchange model of diffusion," *NMR in Biomedicine*, vol. 23, no. 7, pp. 711–724, 2010. [Online]. Available: http://dx.doi.org/10.1002/nbm.1577

PLACE PHOTO HERE

Michael Shell Biography text here.

John Doe Biography text here.

Jane Doe Biography text here.

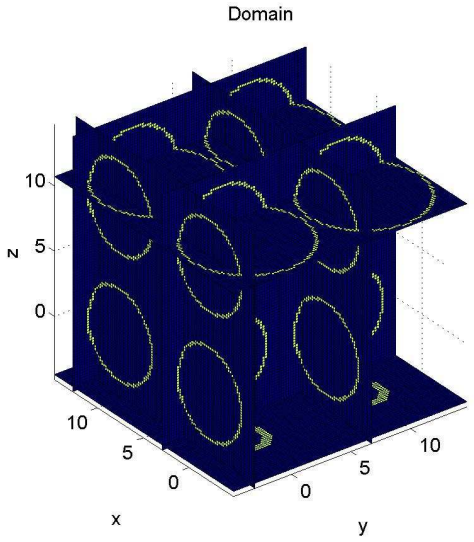

(a) Domain

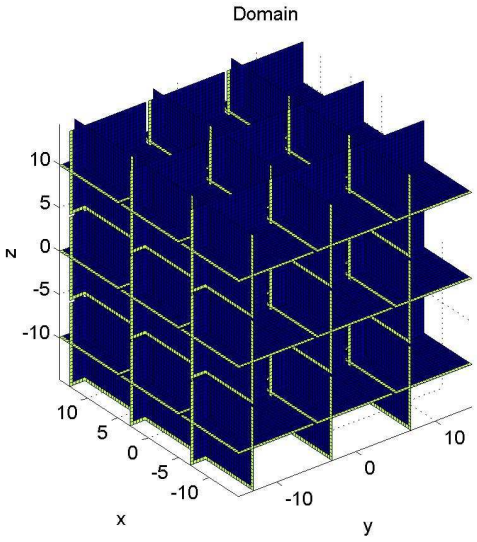

(a) Domain

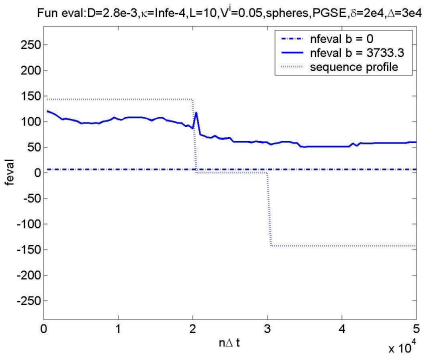

(b) Function evaluations

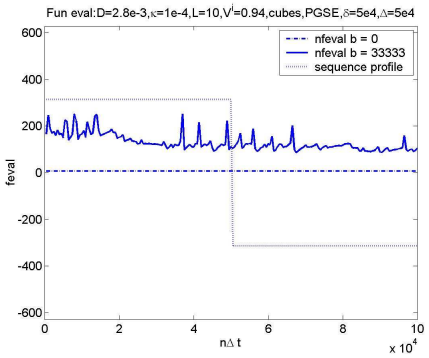

(b) Function evaluations

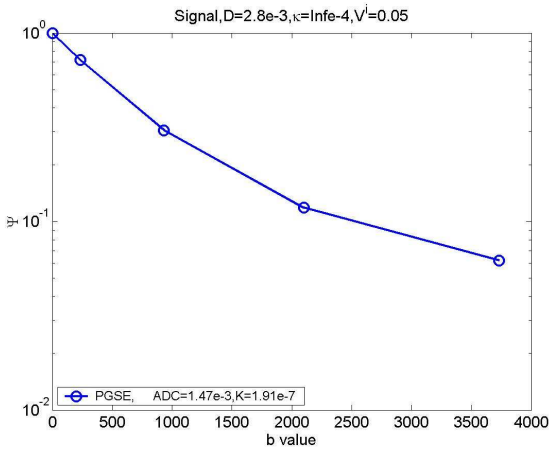

(c) Signal

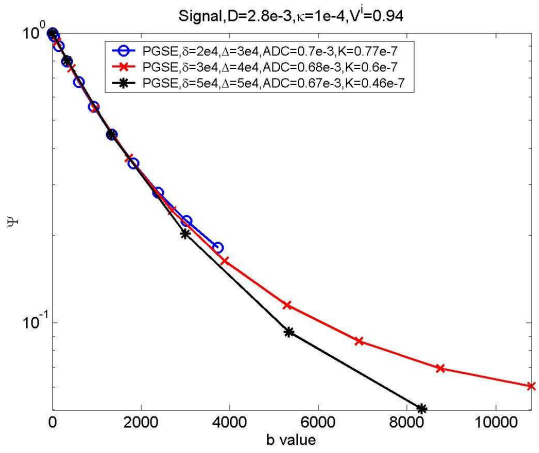

(c) Signal

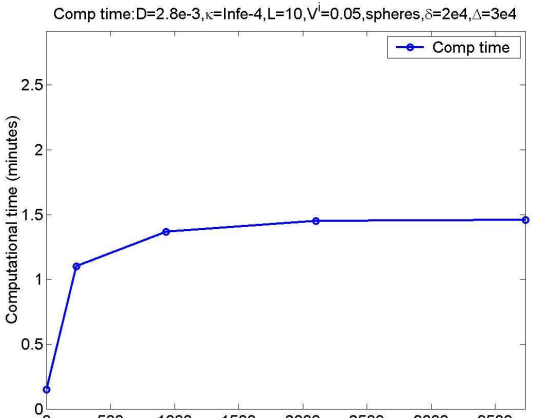

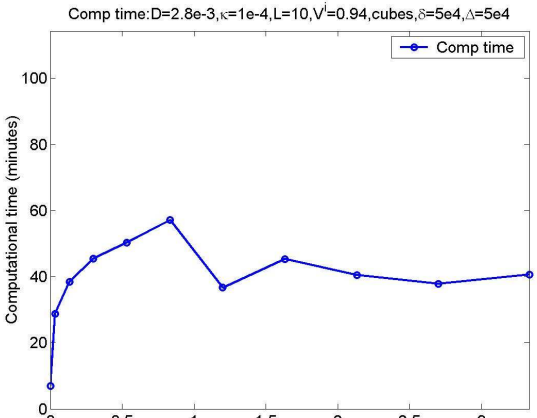

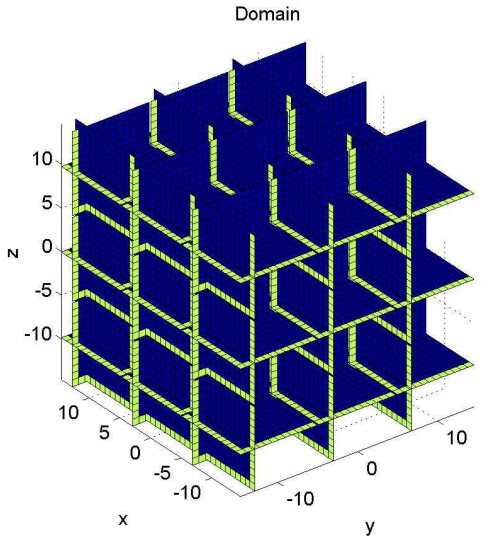

(a) Domain

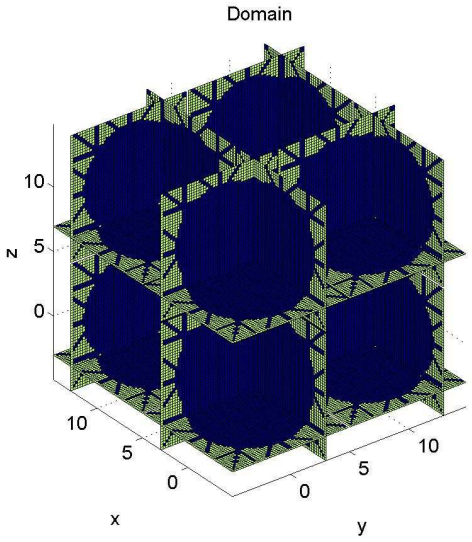

(a) Domain

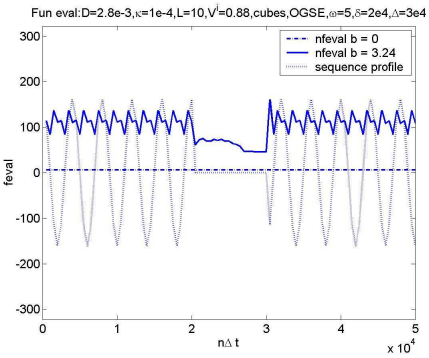

(b) Function evaluations

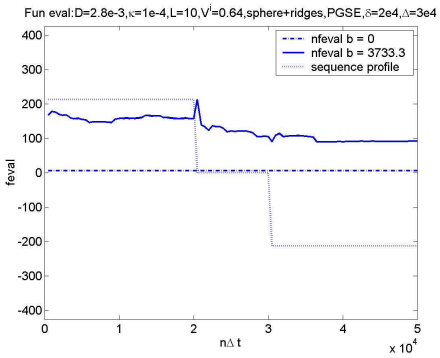

(b) Function evaluations

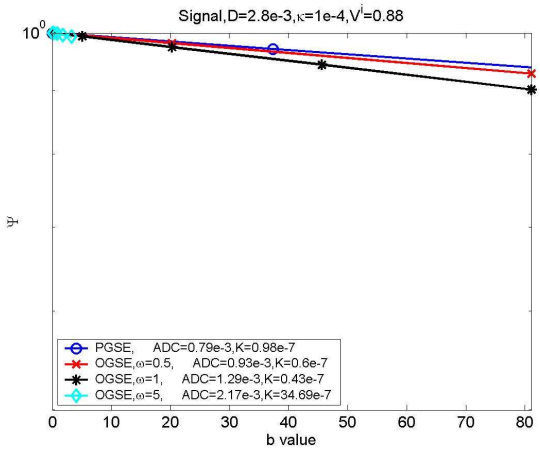

(c) Signal

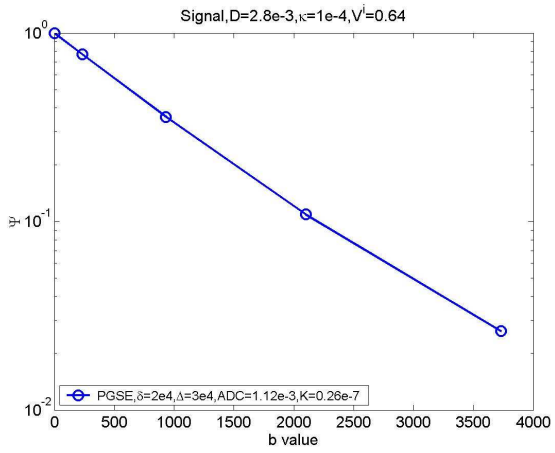

(c) Signal

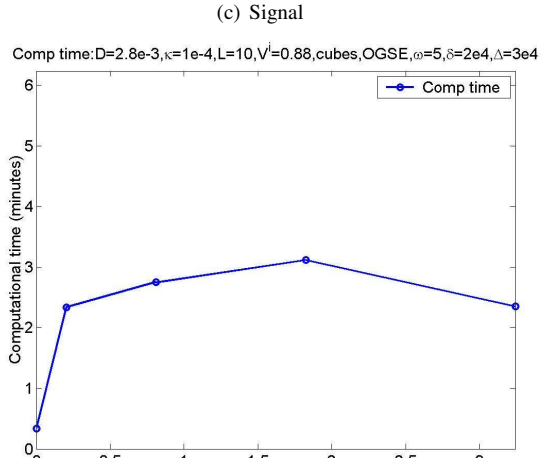

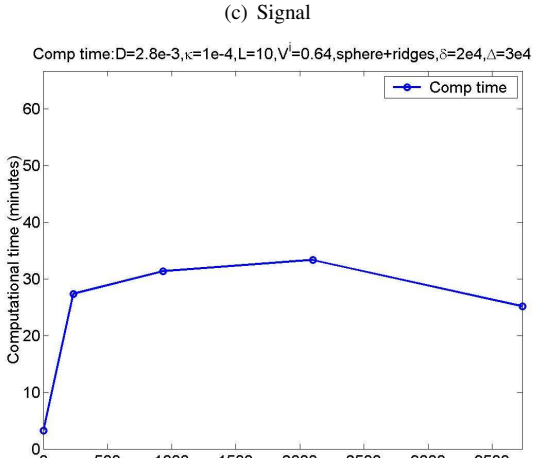

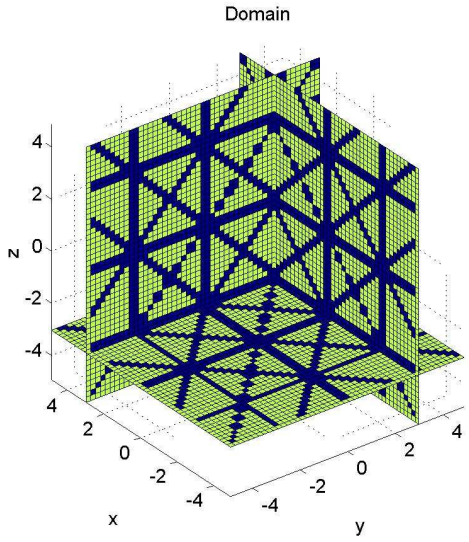

(a) Domain

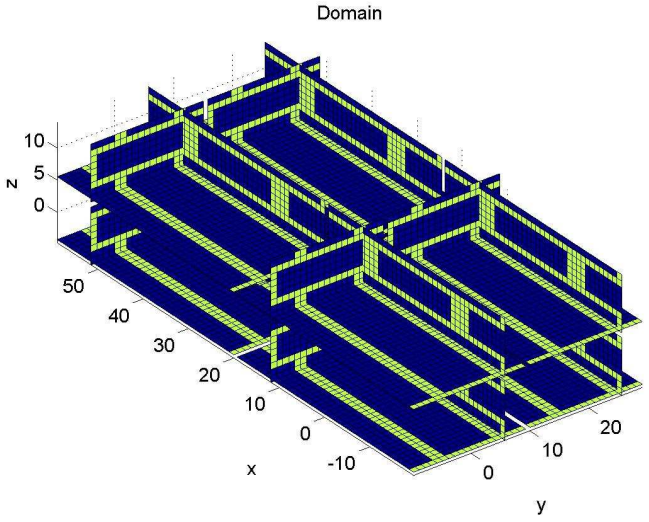

(a) Domain

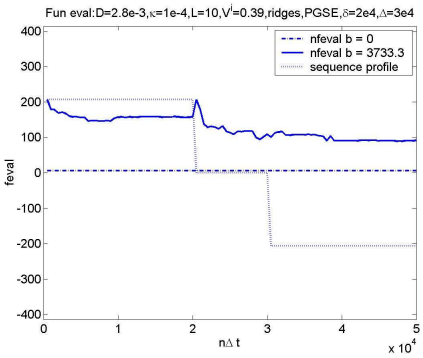

(b) Function evaluations

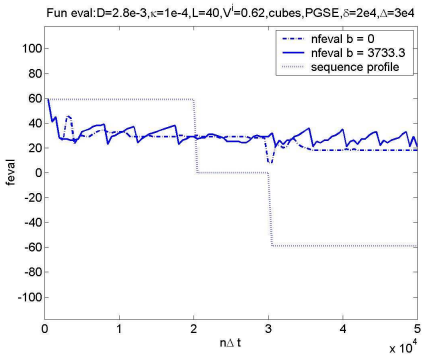

(b) Function evaluations

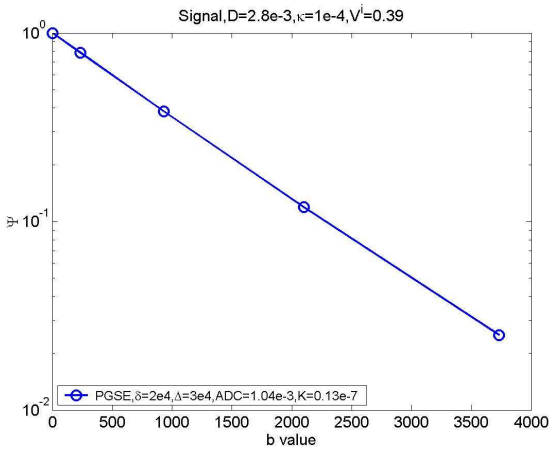

(c) Signal

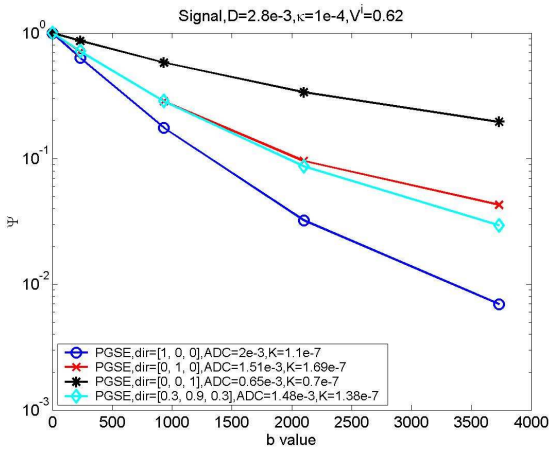

(c) Signal